Bioresource Technology 300 (2020) 122642

Contents lists available at ScienceDirect

Bioresource Technology

journal homepage: www.elsevier.com/locate/biortech

Vitamin-C-enabled reduced graphene oxide chemistry for tuning biofilm phenotypes of methylotrophs on nickel electrodes in microbial fuel cells

Jamil Islam[a,c], Govinda Chilkoor[a,d], Kalimuthu Jawaharraj[a,c], Saurabh Sudha Dhiman[a,b,c], Rajesh Sani[b,c,d], Venkataramana Gadhamshetty[a,c,d,*]

[a] Civil and Environmental Engineering, South Dakota School of Mines and Technology, 501 E. St. Joseph Street, Rapid City, SD 57701, USA
[b] Chemical and Biological Engineering, South Dakota School of Mines and Technology, 501 E. St. Joseph Street, Rapid City, SD 57701, USA
[c] BuG ReMeDEE Consortium, South Dakota School of Mines and Technology, Rapid City, SD 57701, USA
[d] 2-Dimensional Materials for Biofilm Engineering Science and Technology (2DBEST) Center, South Dakota School of Mines and Technology, Rapid City, SD 57701, USA

GRAPHICAL ABSTRACT

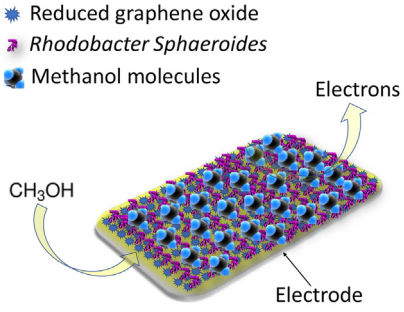

ARTICLE INFO

Keywords:
Biofilm
Electrodes
Graphene
Methylotrophs
Microbial fuel cells

ABSTRACT

This study reports the use of multi-layered reduced graphene oxide (rGO) coating on porous nickel foam (NF) electrodes for enhancing biofilm growth of *Rhodobacter Sphaeroides* spp fed with methanol in microbial fuel cells (CH_3OH-MFCs). Electrochemical methods were used to assess the methylotrophic activity on rGO/NF electrodes. The power density and current density offered by rGO/NF (1200 mW m^{-2} and 680 mA m^{-2}) were 220-fold and 540-fold higher compared to bare NF (5.50 mW m^{-2} and 1.26 mA m^{-2}), respectively. Electrochemical impedance spectroscopy results show that rGO/NF suppresses charge transfer resistance to CH_3OH oxidation by 40-fold compared to the control. This improved performance is due to the ability of rGO coatings to decrease the wetting contact angle (improve the hydrophilicity) of NF from 128^0 to 0^0. A preliminary cost analysis was carried out to assess the viability of rGO/NF electrodes via vitamin-C-enabled graphene oxide chemistry for CH_3OH-MFCs applications.

1. Introduction

The global emissions of methane (CH_4), a potent greenhouse gas has reached ~560 Tera grams per year (Saunois et al., 2016). It is generally agreed that the climate change could be reversed by removing the greenhouse gases from the atmosphere. To reduce the current CH_4 concentration (1,860 ppb) to preindustrial levels (750 ppb), nearly 3.2 Giga tons (Gt) of CH_4 should be removed from the atmosphere (Jackson

* Corresponding author at: Civil and Environmental Engineering, South Dakota School of Mines and Technology, 501 E. St. Joseph Street, Rapid City, SD 57701, USA.
E-mail address: Venkata.Gadhamshetty@sdsmt.edu (V. Gadhamshetty).

https://doi.org/10.1016/j.biortech.2019.122642
Received 1 October 2019; Received in revised form 15 December 2019; Accepted 16 December 2019
Available online 19 December 2019
0960-8524/

et al., 2019). Such a goal requires strategies to harvest CH_4 from the atmosphere and turn it into value-added products. (Latimer et al., 2018; Raynes et al., 2019). Gaseous CH_4 can be converted into methanol (CH_3OH), a suitable precursor to synthesize many products including formaldehyde, formate, single cell proteins and fuels (Bjorck et al., 2018; Strong et al., 2015; Xin et al., 2004).

Given the vast CH_4/CH_3OH reserves it would be beneficial to convert them directly into electricity in microbial fuel cells (MFCs). The prior studies have established the use of MFCs for treating municipal wastewater (Pant et al., 2010), recalcitrant forms of oil and gas wastewater (Shrestha et al., 2017) and complex hemicellulosic wastes (Shrestha et al., 2018). Recent studies have discussed the possibility of using mixed microbial population for treating CH_4 and CH_3OH in MFCs (Logan et al., 2007). The focus of this study is to enable the use of pure cultures of methylotrophs for using reduced carbon substrates such as methanol to generate electricity in MFCs.

Noting that methanotrophs are characterized by slow growth kinetics under anaerobic conditions, it is relatively difficult to grow their electrogenic biofilms (i.e., biofilms that facilitate extracellular electron transfer from methanotrophs to electrodes) using conventional carbonaceous electrodes. Surface modification techniques can be used to tailor desirable surface properties (surface area, surface charge and wettability) of electrodes (Artyushkova et al., 2015) and tune the biofilm growth. In general, biofilms grow well on conductive, rough, hydrophilic and positively charged surfaces (Ye et al., 2013; Guo et al., 2013; Santoro et al., 2015).

This study explored the use of vitamin-C-enabled GO reduction chemistry as a facile method for depositing rGO on 3D porous NF electrodes. The rGO/NF electrodes were then used to grow biofilms of *Rhodobacter Sphaeroides* spp., a previously unexplored methylotroph in CH_3OH-MFCs (methanol: the sole electron donor; rGO/NF: the sole terminal electron acceptor). The electrochemistry tests revealed that rGO/NF electrodes yield 220-fold higher power density and 540-fold higher current density compared to bare NF. Electrochemical impedance spectroscopy results showed that rGO/NF suppresses the charge transfer resistance in CH_3OH-MFCs by 40-fold. Microscopy tests followed by contact angle measurements were used to discern the contributions of rGO layers on the overall improvement to CH_3OH-MFCs. The hydrophilicity of rGO/NF electrodes improved significantly when compared to bare NF. A cost analysis was performed to assess the viability of vitamin-C-assisted GO reduction chemistry for obtaining rGO/NF electrodes for CH_3OH-MFCs applications.

2. Materials and methods

2.1. Materials

Graphene oxide (GO) powder and 3D NF (30 cm × 20 cm) were purchased from Sigma Aldrich, USA and MTI Corporation, USA, respectively. The NF had the following specifications-density (346 g/m^3), ≥ 95% porosity, 80–110 pores per inch, average hole diameters of 0.25 mm and 99.99% purity. Both L-Ascorbic acid (vitamin C) and hydrochloric acid (HCl) were purchased from the Fisher Scientific, USA.

2.2. Electrode preparation and surface modifications

2.5 cm × 2.0 cm NF samples were treated in 6 M HCl. The mixture was sonicated for 10 min to eliminate unwanted foreign particles. The treated NF samples were rinsed thoroughly with deionized water (18.2 MΩ.cm). 6 mg mL^{-1} of GO suspensions were prepared by sonicating the GO powder in deionized water for 1 h. The procedure suggested by Chen et al. (2012) was used to facilitate in-situ deposition of rGO layers on the NF samples. Briefly, the pretreated NF samples were immersed in a GO suspension. The mixture was agitated for 10 mins using a vortex mixer (mini vortexer, VWR) and then sonicated for another 10 mins to fill the micropores of the NF samples with GO. The GO/NF suspension was transferred to a plastic tube (diameter of 3 cm) containing vitamin C solution (3.0 mL of 10 mg mL^{-1}) to facilitate an in-situ synthesis of rGO and its deposition onto NF. The reaction tube was kept undisturbed overnight and then heated at 60 °C for 2 h. After cooling the tube at room temperature, the NF samples were removed and rinsed with deionized water in a repeated manner. Finally, the rGO/NF samples were dried at room temperature prior to use in CH_3OH-MFCs.

2.3. Pure culture of Rhodobacter sphaeroides 2.4.1

Pure cultures of *Rhodobacter sphaeroides* 2.4.1 (RSP) was cultured in Nitrate Mineral Salts (NMS) medium modified with 0.1% methanol. The cultures were exposed to a continuous irradiation of white light spectra (300–750 nm) using a white light lamp (1000 lx) under the shaking conditions (150 rpm; 29 ± 1° C, pH-6.8). Bacterial growth was monitored by measuring the optical absorbance at 600 nm using an Epoch™ Microplate Spectrophotometer (BioTek). Cells grown at the mid-exponential growth phase were used as biocatalyst in CH_3OH-MFCs.

To characterize the growth pattern of RSP, the 1x NMS media was used (pH-6.8) (Murrell et al., 2000). Previously optimized temperature (30 °C) was maintained under the shaking conditions (150 rpm). The RSP cells were purged with methane gas every eight hours to provide carbon source during growth phase. The same procedures were used to grow two model methylotrophs (i.e. *Methylococcus capsulatus* Bath and *Methylosinus trichosporium* OB3b). Experiments were conducted in a 250 mL Erlenmeyer flask containing 100 mL of sterilized media. Operational pH-6.8 was maintained at using 0.1 M NaOH and H_2SO_4. The growth pattern of RSP was assessed by determining the optical density at 600 nm using quartz tubes of the medium at regular intervals (E-supplementary section).

2.4. MFC Design: anode and cathode

The rGO/NF anode and graphite felt cathode (5 cm × 2 cm) were introduced into the anode and cathode compartment of MFCs, respectively. A control MFCs was established using NF as the anode and graphite felt as cathode. The two electrodes were electrically connected using a titanium wire (TEMco, diameter, 0.16002 mm). The projected surface area of anode and cathode were 5 cm^2 and 10 cm^2, respectively. The thickness of NF and graphite felt were 0.16 cm and 0.4 cm, respectively. The anode compartment was filled with 20 mL of the NMS media inoculated with pure culture of RSP cells from the exponential phase. 0.1 M potassium ferricyanide buffered in PBS (pH = 7.0) was used as the catholyte in all of the tests. The anode compartment was exposed to a continuous irradiation of white light using a white light lamp (1000 lx). The test MFCs were configured with rGO/NF electrodes and controls with bare NF electrodes. Both the test CH_3OH-MFCs and controls were operated continuously for seven days in a fed-batch mode using an external load (R_{ext}) of 1000 Ω.

2.5. Electrochemical measurements

The electrochemical impedance spectroscopy (EIS) and cyclic voltammetry (CV) tests were carried out using a Gamry Reference 600 potentiostat and using the procedures described in our earlier study. To discern the contributions of rGO coating to the overall electrochemical performance of rGO/NF electrodes, CV tests were carried out in a three-electrode electrochemical cell using 0.1 M PBS electrolyte (pH-7.0). Pristine NF or rGO/NF were used as the working electrode, and standard platinum electrode (PINE research, USA) and Ag/AgCl as the counter and reference electrode, respectively. These tests were carried out under abiotic conditions. On Day 1 and Day 7, the CV tests were carried out using the CH_3OH-MFCs cell in a two-electrode mode where anode (NF or rGO/NF) and Ag/AgCl were used as the working electrode and reference electrode, respectively. Temporal profiles of the open

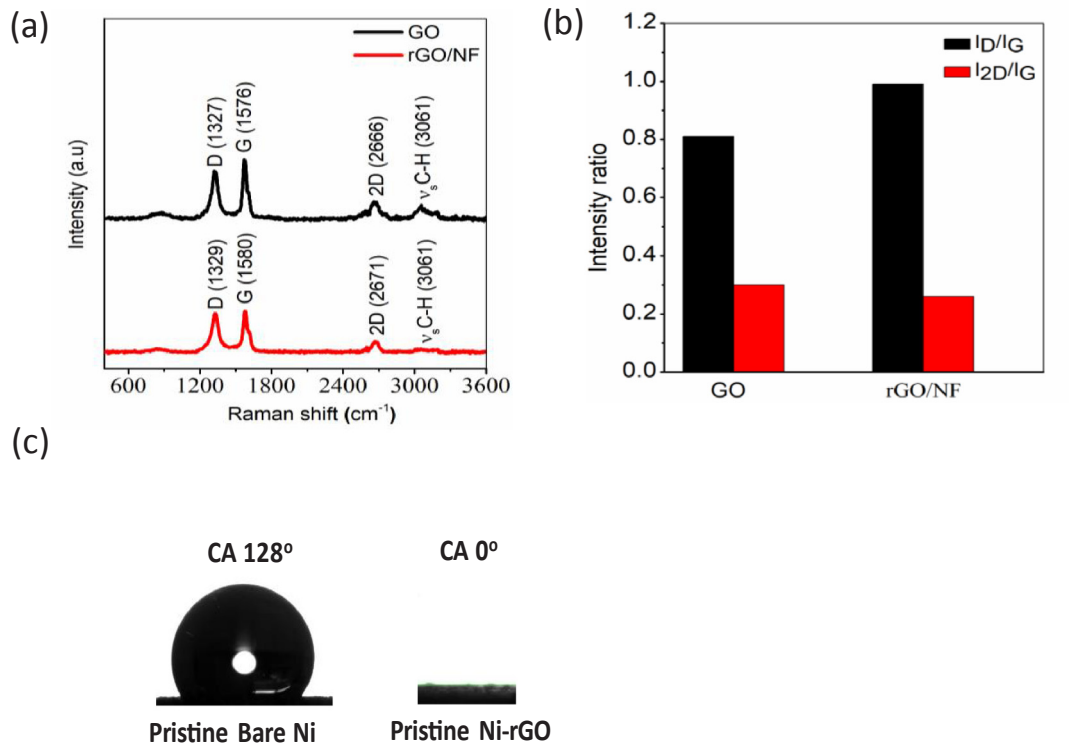

Fig. 1. Materials characterization of NF and rGO/NF. Raman spectra of graphene oxide (GO) and rGO/NF (a). Raman peaks intensity ratio of graphene oxide (GO) and rGO/NF (b). The static water contact angle measurement of pristine bare NF and rGO/NF (c).

circuit voltage (OCV) and electric current were monitored using a personal data acquisition system. A variable resistor box was used to generate the polarization curves by varying the R_{ext} from 1 MΩ to 1 Ω.

To quantify the charge transfer resistance, the impedance data from the Nyquist plot were fitted to an electrical equivalent circuit (EEC) (Fig. 4c) consisting of an ohmic resistance (R_s), two parallel RC circuits (Resistance, R and Capacitance, C) and a Warburg diffusion (W) element. The first RC circuit represents biofilm parameters, specifically the resistance (R_b) and capacitance (C_b) offered by the RSP biofilm on the anode surface. The second RC circuit consists of a charge transfer resistance (R_{ct}) and double layer capacitance (C_{dl}) elements. The capacitance were substituted with constant phase element (CPE) to account for the effects of inhomogeneous surface resulting from the electrode roughness and distributed electrochemical reaction.

2.6. Materials characterization

Detailed morphological characterization and structural properties of GO, NF and rGO/NF samples were carried out using scanning electron microscopy (SEM), Raman spectroscopy and contact angle measurements. The wettability of NF and rGO/NF samples were measured using a goniometer (Model 500, ramé-hart Instrument Co.). DROP-image advanced v2.4 software was used to analyze the attained water droplets for evaluating the contact angle. The morphological analysis of both the NF and rGO/NF samples (without biofilm and with biofilm) were carried out using the Sigma Zeiss SEM. Prior to the SEM observation, the electrodes were fixed using 3% (v/v) glutaraldehyde in a sodium cacodylate buffer (0.1 M, pH-7.2) for 2 h at room temperature. The electrodes were later rinsed with sodium cacodylate buffer solution for three times followed by distilled water. Electrodes were then dehydrated in acetone and dried overnight in a desiccator. Raman spectra were carried out by using ffTA Foram X3 module (Foster + Freeman Ltd, Evesham, UK) using a lens magnification of 10X, laser excitation wavelength of 638 nm and power of 10 mW. The spectrum was collected in the wavenumber range of 400–3700 cm^{-1}.

3. Results and discussion

3.1. R. Sphaeroides as the model biocatalyst in CH_3OH-MFCs

This study used *Rhodobacter sphaeroides* as the model biocatalyst in CH_3OH-MFCs for the following reasons. Based on the analysis of the growth curves, *Rhodobacter sphaeroides* offered higher growth rates compared to the model methylotrophs (*Methylococcus capsulatus* and *Methylosinus trichosporium)* (E-supplementary). A data mining exercise revealed presence of a metal-binding gene (ID: 3720982) on chromosome 1 (NC_007493.2) in the *R. sphaeroides*. Binding of the metal ions will result in cell proliferation and subsequent biofilm formation. Additional tests will be required to confirm the role of annotated genes. However, transition metals ions such as those based on Ni have been reported to stimulate growth of biofilms of Gram-negative microorganisms. A data mining approach was further used to identify the proteins governing interactions among cells. Two genes (gene ID: 3,718,241 and gene ID: 3717932) were shortlisted as candidate proteins that regulates the quorum sensing phenomenon. Expression studies and in-silico analysis are underway for enabling detailed characterization of the identified genes. Based on this background information, a study was designed to assess the ability of rGO/NF electrodes to attach the RSP cells and subsequently promote their biofilm growth in CH_3OH-MFCs.

3.2. Synthesis and characterization of rGO/NF electrodes

The surface properties and chemical properties of rGO were characterized using SEM, Raman spectroscopy and contact angle measurements. The pristine form of NF displayed the typical honeycomb structure at lower magnification and clearly identified grain boundaries at higher magnification. However, rGO/NF displayed a uniformly

covered layer of rGO within the NF network, confirming the in-situ reduction of GO and simultaneous deposition of rGO via dip-coating process. The higher magnification SEM images of rGO/NF revealed the corrugated rGO structure with the vertical edge boundaries (E-supplementary).

The formation of rGO via the vitamin-C-enabled GO reduction was corroborated using Raman spectroscopy tests (Fig. 1a). A significant increase in the value of D/G ratio confirmed the successful reduction of GO to rGO (Bian et al., 2013). Fig. 1a shows that rGO registered a 1.22-fold higher D/G intensity ratio compared to GO (Fig. 1a, b). The presence of small intensity C–H vibrations peaks in rGO/NF spectra (Fig. 1a) suggests that the chemical reduction is incomplete, yielding –OH, –COOH and –CO functional groups on the rGO/NF surface. This reduction process yielded a superhydrophilic rGO/NF electrodes, as demonstrated from the wettability studies (discussed in Section 3.1). The bands around 1325–1340 cm^{-1} and 1575–1580 cm^{-1} for both GO and rGO/NF confirmed the presence of D and G peaks, respectively, which is a typical Raman signature for graphene (Fig. 1a). D band characterizes the presence of vacancies or dislocations in the graphene layer and at the edges, implying the presence of defects in the rGO (Kaniyoor & Ramaprabhu, 2012; Kudin et al., 2008; Kumar et al., 2014; Xu & Cheng, 2013). Similarly, G peak (near 1580 cm^{-1}) is associated with the in-plane vibrations of carbon atoms which are sp^2 hybridized (Kumar et al., 2014; Ni et al., 2008).

The I_{2D}/I_G ratio can be used to decipher the number of graphene layers. The I_{2D}/I_G for rGO/NF (0.26) was 1.15-fold higher compared to GO (0.30), indicating the presence of multi-layer graphene. Generally, rGO prepared by reduction of GO offers low yield because it possesses few layers of graphene (Priyadarsini et al., 2018). Fig. 1b shows the summary of Raman peak intensity ratio of I_D, I_G and I_{2D}.

To understand the impact of rGO coating on the wettability of NF, contact angle measurements were carried out using the sessile drop technique (Fig. 1c). The higher value of the static contact angle for bare NF (128^0) explains its superhydrophobic behavior. Typically, hydrophobic surfaces are characterized with a contact angle greater than 90^0. The literature also suggests that the contact angle for nickel foam could be as high as high as 138^0, primarily due to its porous structure that traps air at the metal/water interface. After coating the NF with rGO, the rGO/NF surface displayed a water contact angle of 0^0 (Fig. 1c). This superhydrophilic nature of rGO/NF is primarily due to the presence of oxygen-rich functional groups which interact with the polar water to increase the overall wettability (Zanin et al., 2014). The lower contact angle typically implies higher spread of the liquid on the surface and thus the lower ability for microorganisms to form a biofilm. However, the nature of bacterial attachment and biofilm formation entirely depends upon the inherent surficial properties of the participating bacteria. A series of prior studies have demonstrated that superhydrophilic electrodes promote bacterial adhesion and biofilm formation compared to hydrophobic surfaces (Choudhury et al., 2017; Cornejo et al., 2015; Guo et al., 2013; Santoro et al., 2015).

As will be discussed in the subsequent sections, the rGO/NF electrodes enhance biofilm growth (See the E-supplementary sections for SEM images) and offers lower impedance when compared to bare NF. These findings suggest that the hydrophilic characteristics of rGO coating increases the contact between the nickel electrode and methanol-supplemented NMS electrolyte, increasing the charge transfer rates and decreasing the overall impedance (Santoro et al., 2015). These results also suggest that the hydrophilic rGO/NF electrodes enable higher power density in CH_3OH-MFCs.

To evaluate the electrocatalytic activity of rGO/NF surfaces, cyclic voltammetry was performed in a three-electrode system using the 0.1 M PBS buffer (pH-7.0). The CV tests were carried out using a scan rate of 100 mVs^{-1} and within the applied voltage range of −1.0 V to 1.0 V (vs. Ag/AgCl). The voltammogram of rGO/NF (Fig. 2) showed a quasi-rectangular area suggesting higher capacitance compared to bare NF. Based on the integration of the area within the CV curves, rGO/NF

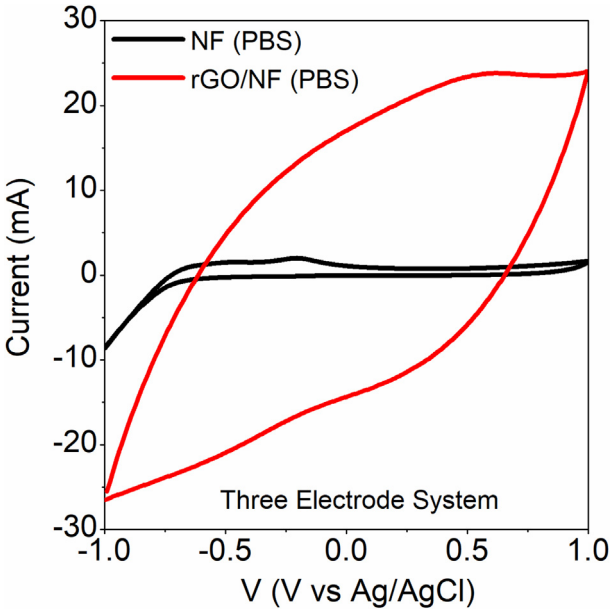

Fig. 2. Electrochemical characterization of NF and rGO/NF by cyclic voltammogram (CV) in potassium buffer solution (0.1 M) in three electrode system.

offered a 10% higher capacitance (74.8 μF/cm^2) compared to NF (68.1 μF/cm^2). These results indicate that the rGO coating increased the effective surface area of the NF electrodes (Xiao et al., 2012; Zhang et al., 2011).

3.3. Biofilm formation and bio-electrochemical performance of rGO/NF versus NF

3.3.1. SEM images reveal more bacterial adhesion on rGO/NF anode

Formation of electroactive biofilms on the rGO/NF anode surface is critical to sustain higher current generation in CH_3OH-MFCs. The SEM tests were used to analyze and compare the growth, morphology and surface coverage of RSP biofilms on the exposed rGO/NF and NF electrodes (See the E-supplementary sections for SEM images). The SEM images revealed higher biofilm density and better biofilm coverage on rGO/NF surface compared to bare NF (E-supplementary). The higher magnification SEM image shown the typical rod-shaped characteristics of RSP.

3.3.2. Higher electrochemical performance of rGO/NF compared to NF electrode

After confirming the denser biofilms of methylotrophs on rGO/NF, extensive investigation of electrical performance was carried out by monitoring the temporal profiles of OCV, power density and current density in CH_3OH-MFCs (Fig. 3a–c). The rGO/NF outperformed NF throughout the CH_3OH-MFCs tests. The rGO/NF offered higher OCV values compared to NF. A higher OCV value infers good interactions between the RSP biofilm and rGO/NF electrodes, which can be expected to enhance bioelectrocatalytic oxidation of methanol. Fig. 3b shows the OCV values for a time span of 6 h on Day 7. The OCV for rGO/NF was 2-fold higher (780 mV vs Ag/AgCl) compared to NF (390 mV vs Ag/AgCl) during the 6 h of fed-batch CH_3OH-MFCs operation. The minimum OCV rGO/NF was 130 mV higher compared to NF (390 mV vs Ag/AgCl). The OCV value for rGO/NF increased from 450 mV vs Ag/AgCl (at t = 0 h) to 780 mV vs Ag/AgCl (at t = 6 h) where it remained constant at 380 mV for NF CH_3OH-MFCs.

Fig. 3c shows the three consecutive RSP inoculating/feeding cycles that lasted for a week of continuous current generation. The average current density in rGO/NF (680 mA m^{-2}) was 540-fold higher compared to NF. An immediate restoration of current generation was

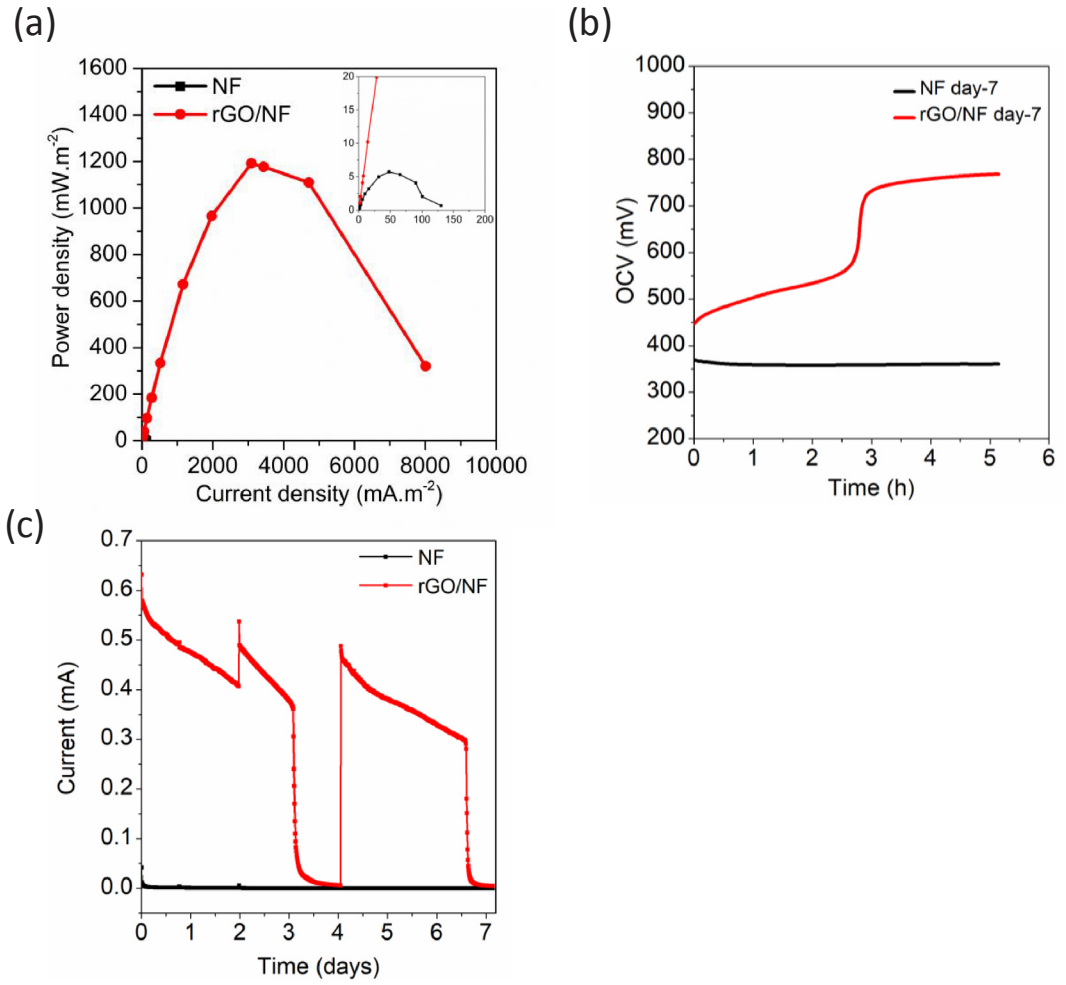

Fig. 3. Higher electrochemical performance of rGO/NF compared to NF electrode. Power density (a), OCV (b), and current (c) for NF and rGO/NF after 7 days of CH_3OH-MFCs operation.

observed after replacing 50% of the spent electrolyte with a fresh NMS medium. The electricity production sustained for another 60 h indicating that CH_3OH-MFCs continued to oxidize methanol to generate electric power. The peak power density of rGO/NF (1200 $mW.m^{-2}$) was also 220-fold higher compared to NF.

3.3.3. Electrochemical impedance

Fig. 4a, b shows the Nyquist plots for NF and rGO/NF on day 1 and day 7, respectively. As shown, the Nyquist plots for CH_3OH-MFCs on Day 1 and Day 7 are significantly different. On both Day 1 and Day 7, the Nyquist plots for rGO/NF displayed extremely smaller semicircle compared to NF, suggesting lower charge transfer resistance and higher reaction kinetics on the rGO/NF surface (Fig. 4). The diameter of semicircle for Nyquist plot on a complex plane consisting of real impedance (x-axis) and imaginary impedance (y-axis) represent the charge transfer resistance. The EIS analysis (Fig. 4a, b) revealed that the charge transfer resistance for rGO/NF was three orders of magnitude lower than bare NF after 7 days of CH_3OH-MFCs operation. This finding confirms the formation of electroactive biofilm on the surface of rGO/NF. The charge transfer resistance on Day 1 for rGO/NF (41.3 $K\Omega.cm^2$) was an order of magnitude lower compared to NF (233 $K\Omega.cm^2$). The corresponding R_b was 2.66-fold lower compared to NF. On Day 7, the R_{ct} value of rGO/NF further dropped by 76% (9.70 $K\Omega.cm^2$) compared to Day 1 (41.3 $K\Omega.cm^2$). Furthermore, at the end of day 7, the R_{ct} values for rGO/NF (9.70 $K\Omega.cm^2$) was three orders of magnitude lower compared to NF (3.34 $M\Omega.cm^2$). The ohmic resistance for rGO/NF showed a 10-fold reduction whereas the NF registered a 2-fold reduction within the 7 days of the fed-batch CH_3OH-MFCs operation. EIS analysis suggested that the rGO/NF enhanced the growth of electroactive biofilm which increased the kinetics of bioelectrochemical oxidation of methanol. As discussed in Section 3.1, the superhydrophilic rGO/NF anode increased the charge transfer rates by facilitating a good contact between the NMS electrolyte and the rGO/NF surface. However, NF anode did not show any significant difference in the impedance values on Day 1 and Day 7. This result confirms that the NF did not promote the growth of RSP biofilms. The findings from these EIS tests collaborate with SEM analysis where enhanced biofilm formation was observed in rGO/NF compared to NF (E-supplementary).The presence of rGO on 3D-NF provides a larger surface area for biofilm formation and effective diffusion of growth medium into the macro porous scaffold.

3.3.4. Voltammetry tests

In order to understand the methanol oxidation pathways occurring on the surface of NF and rGO/NF in CH_3OH-MFCs, CV was carried out in 100 mM potassium buffer solution (pH-7.0) in a three-electrode system (Fig. 2) and in CH_3OH-MFCs (Fig. 5). The two oxidation peaks for rGO/NF electrode occurring at −0.045 V and 0.24 V (vs. Ag/AgCl) in the forward scan suggest that the methanol potentially oxidized to formaldehyde. Beyond the forward scan potential of 0.5 V, the rGO/NF did not show any oxidation peak (Jarvi et al., 1997; Korzeniewski & Childers, 1998). In contrast, the CV for NF anode showed oxidation peaks corresponding to CH_3OH oxidation to formaldehyde (0.24 V vs Ag/AgCl) and further oxidation of formaldehyde (> 0.5 V) into formate which subsequently oxidized into CO_2 (Iwasita and Vielstich, 1986; Ota

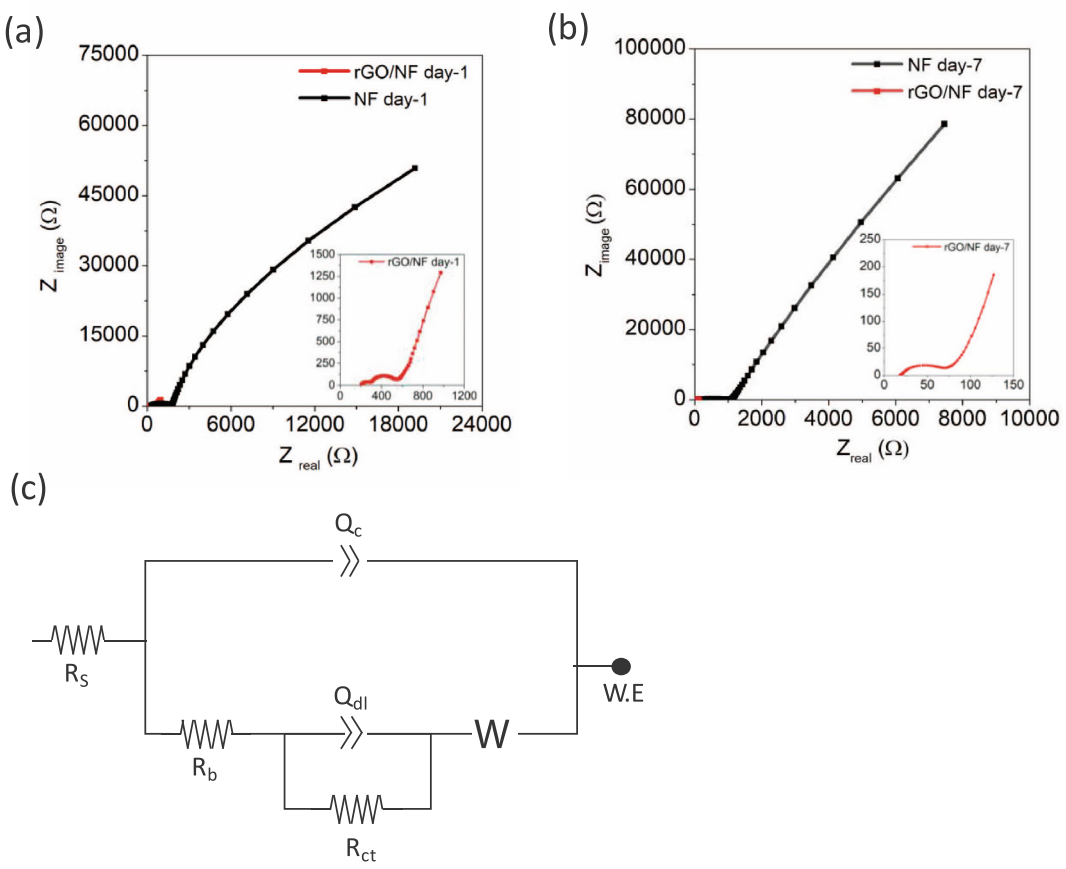

Fig. 4. Measurement of electrochemical impedance (EIS) of NF and rGO/NF at day 1 (a) and day 7 (b). Electrical equivalent circuit (EEC) of NF CH_3OH-MFCs and rGO/NF CH_3OH-MFCs (c).

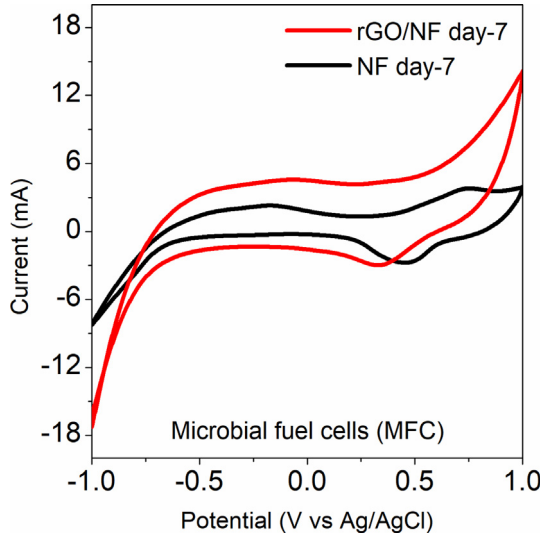

Fig. 5. Cyclic voltammogram (CV) of NF CH_3OH-MFCs and rGO/NF CH_3OH-MFCs on day 7 of CH_3OH-MFCs operation.

et al., 1984). The CV results suggest that the rGO coating on NF has potentially helped methanotrophs to alter the CH_3OH oxidation pathway to a single step reaction to form formaldehyde product, and without forming other by-products. Further, the oxidation current density of rGO/NF electrode was 12.5-fold higher compared to bare NF, indicating the enhanced electroactive surface area. These results suggest that rGO coating enhances the biocatalytic property of NF electrodes (Shibata & Motoo, 1986).

3.3.5. Cost analyses

A unique combination of functional properties of rGO/NF electrodes render them beneficial in CH_3OH-fed bioelectrochemistry applications. To realize their full potential for practical applications, it is important to produce high quality rGO material on a large scale at low cost and in a reproducible manner. This study explored the use of vitamin-C-enabled-graphene-oxide reduction chemistry as a cost-effective method for synthesizing rGO (Chen et al., 2012) and depositing it on NF electrodes. A preliminary cost analyses was carried out for rGO/NF electrode using 1 cm^2 of NF as the baseline case. A comprehensive details of vendor and unit cost for the raw materials used to synthesize rGO and for depositing it on NF electrodes (E-supplementary). The cost analysis was based on the use of an improved Hummer's method for synthesizing GO (Marcano et al., 2010). To enable cost analyses of the surface modification method for achieving rGO/NF electrodes at a fundamental level, a segment-by-segment calculation method was used. The cost estimated for 1 cm^2 of NF was 12 cents and lion share of the manufacturing cost went to NF that was 67.15%. The contributions of the cost of the surface modifier (GO) was determined to be 12.46% whereas the pretreatment cost for NF was 19.34%. Most remarkably, Vitamin-C, the reducing agent contributed to only 0.68% of the total costs. The cost of rGO/NF electrodes ($0.12/$cm^2$) established in this study was 55-fold lower compared to commercially available graphene/nickel electrodes (Graphene_Supermarket).

4. Conclusions

This study demonstrated a facile approach to homogenously coat a layer of reduced graphene (rGO) oxide on 3D nickel electrodes. The in-situ reduction method yielded a superhydrophilic electrode that enhanced the attachment of methylotrophic cells and subsequently their

biofilm growth. The biocompatible rGO/NF electrodes enabled a 220-fold and 540-fold higher power density and current density, respectively when compared to bare NF electrode. A preliminary cost analysis indicates a promise to develop an inexpensive manufacturing process to obtain high performance rGO/NF electrodes for methanol-fed microbial fuel cells.

CRediT authorship contribution statement

Jamil Islam: Conceptualization, Methodology, Investigation, Writing - original draft. **Govinda Chilkoor:** Validation, Writing - review & editing. **Kalimuthu Jawaharraj:** Writing - review & editing, Resources, Validation. **Saurabh Sudha Dhiman:** Writing - review & editing, Resources. **Rajesh Sani:** Funding acquisition, Project Administration. **Venkataramana Gadhamshetty:** Conceptualization, Methodology, Supervision, Project administration, Writing - review & editing, Funding acquisition.

Declaration of Competing Interest

The authors declare that they have no known competing financial interests or personal relationships that could have appeared to influence the work reported in this paper.

Acknowledgements

Gadhamshetty acknowledges the funding support from the National Science Foundation (NSF). BuGReMeDEE Award (# 1736255), NASA, (NNX16AQ98A), and in part by the NSF RII Track-1: Building on The 2020 Vision: Expanding Research, Education and Innovation in SD (#1849206)

Appendix A. Supplementary data

Supplementary data to this article can be found online at https://doi.org/10.1016/j.biortech.2019.122642.

References

Artyushkova, K., Cornejo, J.A., Ista, L.K., Babanova, S., Santoro, C., Atanassov, P., Schuler, A.J., 2015. Relationship between surface chemistry, biofilm structure, and electron transfer in Shewanella anodes. Biointerphases 10, 019013.

Bian, S., Scott, A.M., Cao, Y., Liang, Y., Osuna, S., Houk, K., Braunschweig, A.B., 2013. Covalently patterned graphene surfaces by a force-accelerated Diels-Alder reaction. J. Am. Chem. Soc. 135, 9240–9243.

Bjorck, C.E., Dobson, P.D., Pandhal, J., 2018. Biotechnological conversion of methane to methanol: evaluation of progress and potential. AIMS Bioeng. 5, 1–38.

Chen, J., Sheng, K., Luo, P., Li, C., Shi, G., 2012. Graphene hydrogels deposited in nickel foams for high-rate electrochemical capacitors. Adv. Biomater. 24, 4569–4573.

Choudhury, A., Barbora, L., Arya, D., Lal, B., Subudhi, S., Mohan, S.V., Ahammad, S.Z., Verma, A., 2017. Effect of electrode surface properties on enhanced electron transfer activity in microbial fuel cells. Eng. Life Sci. 17, 186–192.

Cornejo, J.A., Lopez, C., Babanova, S., Santoro, C., Artyushkova, K., Ista, L., Schuler, A.J., Atanassov, P., 2015. Surface modification for enhanced biofilm formation and electron transport in Shewanellan anodes. J. Electrochem. Soc. 162, H597–H603.

Guo, K., Freguia, S., Dennis, P.G., Chen, X., Donose, B.C., Keller, J., Gooding, J.J., Rabaey, K., 2013. Effects of surface charge and hydrophobicity on anodic biofilm formation, community composition, and current generation in bioelectrochemical systems. Environ. Sci. Technol. 47, 7563–7570.

Graphene_Supermarket, https://graphene-supermarket.com/3D-Multilayer-Graphene-Film-on-Nickel-Foam-2-x4-3D-Ni-G-Foam-2x4.html. Last accessed. 11.29.2019.

Jackson, R., Solomon, E., Canadell, J., Cargnello, M., Field, C., 2019. Methane removal and atmospheric restoration. Nat. Sustainability 1.

Iwasita, T., Vielstich, W., 1986. On-line mass spectroscopy of volatile products during methanol oxidation at platinum in acid solutions. J. Electroanal. Chem. Interfacial Electrochem. 201 (2), 403–408. https://doi.org/10.1016/0022-0728(86)80064-X.

Jarvi, T., Sriramulu, S., Stuve, E., 1997. Potential dependence of the yield of carbon dioxide from electrocatalytic oxidation of methanol on platinum (100). J. Phys. Chem. B. 101, 3649–3652.

Kaniyoor, A., Ramaprabhu, S., 2012. A Raman spectroscopic investigation of graphite oxide derived graphene. Aip Adv. 2, 032183.

Korzeniewski, C., Childers, C.L., 1998. Formaldehyde yields from methanol electrochemical oxidation on platinum. J. Phys. Chem. B. 102, 489–492.

Kudin, K.N., Ozbas, B., Schniepp, H.C., Prud'Homme, R.K., Aksay, I.A., Car, R., 2008. Raman spectra of graphite oxide and functionalized graphene sheets. Nano lett. 8, 36–41.

Kumar, R., Mehta, B.R., Bhatnagar, M., Ravi, S., Mahapatra, S., Salkalachen, S., Jhawar, P., 2014. Graphen as a transparent conducting and surface field layer in planar Si solar cells. Nanoscale Res. Lett. 9, 349.

Latimer, A.A., Kakekhani, A., Kulkarni, A.R., Nørskov, J.K., 2018. Direct methane to methanol: the selectivity–conversion limit and design strategies. ACS Catal. 8, 6894–6907.

Logan, B., Cheng, S., Watson, V., Estadt, G., 2007. Graphite fiber brush anodes for increased power production in air-cathode microbial fuel cells. Environ. Sci. Technol. 41, 3341–3346.

Marcano, D.C., Kosynkin, D.V., Berlin, J.M., Sinitskii, A., Alemany, L.B., Lu, W., Tour, J.M., 2010. Improved synthesis of graphene oxide. ACS Nano. 4, 4806–4814.

Murrell, J.C., Gilbert, B., McDonald, I.R., 2000. Molecular biology and regulation of methane monooxygenase. Arch. Microbiol. 173, 325–332.

Ni, Z., Wang, Y., Yu, T., Shen, Z., 2008. Raman spectroscopy and imaging of graphene. Nano Res. 1, 273–291.

Ota, K.-I., Nakagawa, Y., Takahashi, M., 1984. Reaction products of anodic oxidation of methanol in sulfuric acid solution. J. Electroanal. Chem. Interfacial Electrochem. 179 (1–2), 179–186. https://doi.org/10.1016/S0022-0728(84)80286-7.

Pant, D., Van Bogaert, G., Diels, L., Vanbroekhoven, K., 2010. A review of the substrates used in microbial fuel cells (MFCs) for sustainable energy production. Bioresour. Technol. 101, 1533–1543.

Priyadarsini, S., Mohanty, S., Mukherjee, S., Basu, S., Mishra, M., 2018. Graphene and graphene oxide as nanomaterials for medicine and biology application. J. Nanostruct. Chem. 8, 123–137.

Raynes, S.J., Shah, M.A., Taylor, R.A., 2019. Direct conversion of methane to methanol with zeolites: towards understanding the role of extra-framework d-block metal and zeolite framework type. Dalton Transactions.

Santoro, C., Babanova, S., Artyushkova, K., Cornejo, J.A., Ista, L., Bretschger, O., Marsili, E., Atanassov, P., Schuler, A.J., 2015. Influence of anode surface chemistry on microbial fuel cell operation. Bioelectrochemistry 106, 141–149.

Saunois, M., Bousquet, P., Poulter, B., Peregon, A., Ciais, P., Canadell, J.G., Dlugokencky, E.J., Etiope, G., Bastviken, D., Houweling, S., 2016. The global methane budget 2000–2012. Earth Syst. Sci. Data 8, 697–751.

Shibata, M., Motoo, S., 1986. Electrocatalysis by ad-atoms: part XX. Rate-determining step in methanol oxidation enhanced by oxygen-adsorbing ad-atoms. J. Electroanal. Chem. Interfacial Electrochem. 209, 151–158.

Strong, P.J., Xie, S., Clarke, W.P., 2015. Methane as a resource: can the methanotrophs add value? Environ. Sci. Technol. 49, 4001–4018.

Shrestha, N., Govinda, C., Xia, L., Alvaravo, C., Kilduff, J.E., Keating, J.J., Belfort, G., Gadhamshetty, V., 2017. Integrated membrane and microbial fuel cell technologies for enabling energy-efficient effluent Re-use in power plants. Water Res. 117, 37–48.

Shrestha, N., Govinda, C., Vemuri, B., Rathinam, N., Sani, R.K., Gadhamshetty, V., 2018. Extremophiles for microbial-electrochemistry applications: a critical review. Bioresour. Technol. 255, 318–330.

Xiao, L., Damien, J., Luo, J., Jang, H.D., Huang, J., He, Z., 2012. Crumpled graphene particles for microbial fuel cell electrodes. J. Power Sources. 208, 187–192.

Xin, J.-Y., Cui, J.-R., Niu, J.-Z., Hua, S.-F., Xia, C.-G., Li, S.-B., Zhu, L.-M., 2004. Production of methanol from methane by methanotrophic bacteria. Biocatal. Biotransform. 22, 225–229.

Xu, L., Cheng, L., 2013. Graphite oxide under high pressure: a Raman spectroscopic study. J. Nanomater 47.

Ye, Z., Hou, J., Ellis, M.W., Behkam, B., 2013. Effect of anode surface roughness on power generation in microbial fuel cells. In: ASME 2012 International Mechanical Engineering Congress and Exposition. American Society of Mechanical Engineers Digital Collection, pp. 1409–1414.

Zanin, H., Saito, E., Ceragioli, H., Baranauskas, V., Corat, E., 2014. Reduced graphene oxide and vertically aligned carbon nanotubes superhydrophilic films for supercapacitors devices. Mater. Res. Bull. 49, 487–493.

Zhang, Y., Mo, G., Li, X., Zhang, W., Zhang, J., Ye, J., Huang, X., Yu, C., 2011. A graphene modified anode to improve the performance of microbial fuel cells. J. Power Sources. 196, 5402–5407.

Graphene_Supermarket, https://graphene-supermarket.com/3D-Multilayer-Graphene-Film-on-Nickel-Foam-2-x4-3D-Ni-G-Foam-2x4.html.